High Pt Utilization Electrodes for Polymer Electrolyte Membrane Fuel Cells by Dispersing Pt Particles Formed by a Preprecipitation Method on Carbon "Polished" with Polypyrrole

ARTICLE *in* THE JOURNAL OF PHYSICAL CHEMISTRY C · SEPTEMBER 2010

Impact Factor: 4.77 · DOI: 10.1021/jp104664t

4 AUTHORS:

Sreekuttan M. Unni
CSIR - National Chemical Laboratory, Pune
25 PUBLICATIONS **353** CITATIONS
SEE PROFILE

Vishal Mahesh Dhavale
Tokyo Institute of Technology
15 PUBLICATIONS **128** CITATIONS
SEE PROFILE

Vijayamohanan K Pillai
CSIR- CECRI, Central Electrochemical Rese…
241 PUBLICATIONS **5,961** CITATIONS
SEE PROFILE

Sreekumar Kurungot
CSIR - National Chemical Laboratory, Pune
112 PUBLICATIONS **1,389** CITATIONS
SEE PROFILE

High Pt Utilization Electrodes for Polymer Electrolyte Membrane Fuel Cells by Dispersing Pt Particles Formed by a Preprecipitation Method on Carbon "Polished" with Polypyrrole

Sreekuttan M. Unni, Vishal M. Dhavale, Vijayamohanan K. Pillai, and Sreekumar Kurungot*

Physical and Materials Chemistry Division, National Chemical Laboratory, Pune, India

Received: May 21, 2010; Revised Manuscript Received: July 16, 2010

Pt utilization on carbon black (CB) has been significantly improved by initially utilizing polypyrrole (PPy) as a moiety to "polish" the carbon surface and subsequently by dispersing Pt particles formed by a preprecipitation process to minimize their migration into the geometrically restricted areas of the carbon surface. This process strategy has helped to significantly extend the triple-phase boundary as a greater number of Pt particles comes in direct contact with Nafion, leading to a substantial improvement in the overall catalyst utilization. Preliminary analyses such as IR, thermogravimetric analysis, and N_2 sorption confirmed the presence of PPy on the surface. Approximately 50% reduction in the surface area of CB after the controlled in situ polymerization of pyrrole monomer on the carbon surface indicated preferential filling and coverage of pores and other geometrically restricted pockets of carbon surface. On the other hand, by converting Pt into colloids in the preprecipitation method prior to their reduction, the platinum particles are forced to stay on the hybrid support; a major part of which otherwise would have been migrated into the surface pores and defect sites. Platinum particle size on these hybrid supports is 2 times higher than the catalyst prepared by polyol process. However, the electroactive surface area and mass activity are 2 times higher than that of the Pt particles prepared by polyol on hybrid material and are also significantly higher than that of the conventional electrocatalysts prepared by the polyol method. At 0.8 V, the kinetic current density (j_k) of Pt/C-PPy-Pre obtained from the Koutecky−Levich plot is 1.5 and 2.5 times higher than that of catalysts prepared by the polyol method on PPy-coated carbon and Vulcan XC-72 carbon, respectively. Almost 210 and 160 mW cm^{-2} improvement for the maximum power density, respectively with oxygen and air, was obtained with the modified system in comparison to the conventional system when the single cell evaluations were carried out at 60 °C with a Pt loading of 0.5 mg cm^{-2} in the anode and cathode sides. This enhancement in the cell performance under the two different oxygen partial pressure conditions clearly emphasizes the improved oxygen reduction reaction (ORR) and mass-transfer characteristics of the hybrid electrode material compared to the other catalysts.

1. Introduction

As a versatile energy generation technology to effectively meet the stringent environmental norms, polymer electrolyte membrane fuel cells (PEMFCs) have gained significant attention in the last few decades. Technically, among various alternate energy sources, PEMFCs have been considered as ideal systems to serve as power sources for both stationary and mobile applications. To improve the commercial viability and customer acceptance, there are widespread scientific efforts to overcome hurdles such as cost and durability along with the continuous efforts to improve the performance characteristics. Therefore, a breakthrough in the commercialization aspects of PEMFCs will depend largely on how effectively and when the persisting scientific as well as technical challenges mostly in materials can be addressed. Since the sluggish oxygen reduction kinetics in the cell reaction compels one to consider platinum or platinum alloys as the only practical choice, the issue of addressing the cost targets is emerging as a real stumbling block in the path of PEMFC research and development efforts. Even though a variety of materials have been synthesized and tested for the oxygen reduction reaction (ORR), most of the systems fail to simultaneously meet the requirements for cost, activity, and durability. Unless some miraculous innovation happens in the near future, the incremental progress in the development of a non-Pt electrocatalyst for oxygen reduction points toward the inevitable dependency on Pt for this purpose at least for a few more decades.[1−3] In this context, along with the strive for developing effective non-Pt electrocatalysts, it is highly important to develop appropriate strategies to reduce platinum content and maximize platinum utilization in the electrodes. Any petite improvement in this perspective will help to make new benchmarks on Pt-based PEMFCs in terms of both cost and performance. There are recent reports on low Pt loadings (μg level/cm^2) that give very good fuel cell performances.[4,5] However, in such cases also, the Pt utilization in PEMFCs lies at a significantly low level (20−35%) due to the lack of proper interaction of catalyst, catalyst support, and binder at the triple-phase boundary (TPB).[6] Electron as well as proton conductivity of support material and the method of preparation of catalyst are also contributing decisive roles in the overall fuel cell performance.

An ideal catalyst support should be able to perform multiple functions simultaneously in time. The material should be able to show electron and proton conductivity simultaneously. At the same time, it should display high specific surface area and porosity along with good stability in acid media under the operating conditions and electrochemical environment inside the

* To whom correspondence should be addressed. E-mail: k.sreekumar@ncl.res.in. Fax: +91-20-25902636. Tel: +91-20-25902566.

10.1021/jp104664t
Published on Web 08/06/2010

cell. Apart from the above-mentioned properties of the catalyst support, the morphology of the support should help to achieve high Pt (or any other active species) dispersion, utilization, activity, and stability of the catalyst particles as well.[7,8] Among the various catalyst supports (organic, inorganic, hybrid materials) available, carbon black (CB) is considered to be more important because of its high surface area and good electronic conductivity along with its low cost compared to other allotropes of carbon and conducting metal oxides.[7−10] However, there are a few significant issues that question the credibility of CB in the main stream as a support material in fuel cells. For example, CBs generally achieve high surface area through multiple postsynthesis treatments in order to improve surface roughness, porosity, and controlled pore size distribution. The micro- and mesopores inherently present and created by virtue of the postsynthesis treatments together with the general irregularities of the carbon surface create geometric complexities to disperse Pt selectively on the surface and subsequently to establish the TPB around the dispersed Pt nanoparticles. The pores and other geometrically restricted areas on CB can virtually swallow a significant amount of Pt nanoparticles, without allowing the ionomer molecules to interact and form TPB. Moreover, the defects present on the surface of carbon serve as active regions to initiate electrodegradation of carbon, leading to a reduction in the lifetime of PEMFCs.[11] Some reports also show that platinum nanoparticles can accelerate carbon corrosion.[12] In this perspective, our group has been involved in developing carbon-based hybrid materials to take care of the aforementioned issues of CBs, while retaining their excellent morphological characteristics suitable for serving as support materials. To date, a large number of hybrid materials based on carbon have been reported. Inorganic material such as niobium oxide and silica are used for carbon-based hybrid materials as catalyst supports for PEMFC electrodes.[13,14] However, conducting polymer (CP)-based hybrid materials are unique in this respect because of their special properties such as good electronic and protonic conductivity, dispensability, adequate control of their size growth, and flexibility for processing.[7] Among different CPs, materials such as polypyrrole (PPy) and polyaniline as the catalyst support materials have shown promising fuel cell efficiency.[15,16] PPy is unique among the conjugated polymer family since its doping level can be readily controlled through acid doping or base dedoping.[17] It has been shown that the use of macromolecular proton acid as dopant can enhance electric conductivity of PPy and limit the growth of the PPy particle. The hybrid materials prepared from both carbon and PPy have special properties toward electrocatalytic performance originated by their mutual assistance in the composite structure. An important drawback of CP-based catalysts for fuel cell applications is the progressive reduction in performance owing to the migration of Pt particles into the CP matrix; the swelling−drying cycle and voltage fluctuation assist the migration rate.[18−20] Along with this, solvent-assisted Pt dispersion processes such as the polyol process and one-pot synthesis approach generally lead to Pt ionic migration into the polymer matrix, which ultimately can be reduced as metallic Pt particles upon the reduction process.

Here, we report the effective utilization of PPy to "polish" the CB surface by controlled growth of CP on the surface of CB to fill or cover the geometrically restricted portions of the substrate surface (C-PPy). This approach helps to control the porosity of the carbon and thereby to maintain a relatively smooth surface and increased metal availability for the electrode reaction. At the same time, the presence of a carbon backbone in our C-PPy hybrid system effectively prevents the swelling of the thin PPy layer formed on its surface and in the pores. This is in sharp contrast to stability using PPy as an electrocatalytic support.[21] Most importantly, in order to further enhance the level of surface deposition of Pt, a preprecipitation method has been adopted as a unique strategy to circumvent the aforementioned problems of burying Pt particles. In this approach, the Pt ions adsorbed on the C-PPy hybrid are subjected to precipitation followed by reduction by effectively preventing penetration of nanoparticles in the polymer matrix and micropores present on the carbon surface. Along with this, we have taken special care to maintain the PPy content in the minimum possible level to serve merely as a pore-filler and a phase to form a thin layer to maintain surface smoothness. These Pt supported C-PPys by preprecipitation (Pt/C-PPy-Pre) show higher catalytic activity and Pt utilization compared to Pt on carbon by preprecipitation (Pt/C-Pre) and Pt on carbon (Pt/C-Pol) and C-PPy (Pt/C-PPy-Pol), both prepared by the conventional polyol method.

2. Experimental Section

2.1. Preparation of PPy-Loaded Carbon Black (CB) (C-PPy) Substrate. For the preparation of C-PPy hybrid material, functionalized Vulcan XC-72 carbon (F-C) was used as the core support. Instead of executing functionalization using strong acids, chemical pretreatment with H_2O_2 was carried out to prevent any large order surface deformation of the support (F-C). The pretreatment process involved initial treatment of pristine carbon (CABOT Corp., U.S.A.) with 30% H_2O_2 for 5−6 h at 60 °C followed by overnight treatment of the reaction mixture under ambient conditions. C-PPy hybrid material was prepared as reported elsewhere in the literature.[7,18] In the present study, a carbon slurry for the preparation of hybrid was made by mixing 500 mg of F-C and 0.25 mL of glacial acetic acid in 150 mL of deionized (DI) water with a homogenizer. A 100 mg portion of pyrrole was added to the slurry with continuous stirring. Subsequently, 3 mL of 10% H_2O_2 solution was added to the CB slurry, and stirring was continued at room temperature for 1−3 h for polymerizing the monomer. The C-PPy dispersion was filtered, washed with warm deionized water, and dried at 90 °C under vacuum for 6 h.

2.2. Preparation of Pt/CPPy by Preprecipitation Method. For the preparation of the Pt-dispersed C-PPy catalyst, a modified preprecipitation method was adopted.[22] Briefly, for the preparation of 20 wt % Pt catalyst, 400 mg of C-PPy was impregnated with 13 mL of 0.4 M H_2PtCl_6 solution for 2 h in order to ensure that most of the Pt ions were adsorbed onto C-PPy. Subsequently, 100 mL of 10 M NH_4Cl solution was added into the suspension with stirring. This led to the precipitation of Pt ions adsorbed on C-PPy due to the formation of $(NH_4)_2PtCl_6$. The suspension was continuously stirred for 1 h at 80 °C while maintaining the pH at 9.2 for the complete precipitation. With the dropwise addition of 600 mL of 0.2 M $NaBH_4$ at 80 °C for 3 h, $(NH_4)_2PtCl_6$ was reduced to Pt particles adsorbed onto C-PPy. Subsequently, the suspension was filtered and washed with hot triply distilled water to ensure the removal of Cl^- ions. Finally, the catalyst was dried in an air oven at 110 °C for 4 h (Pt/C-PPy-Pre). For comparison, a 20 wt % Pt/C catalyst (Pt/C-Pre) was also prepared using F-C instead of C-PPy, adopting the same method as described above. For the effective comparison of the catalysts prepared using different methods, a 20 wt % Pt supported carbon catalyst was prepared using the conventional polyol method (Pt/C-Pol) as reported elsewere.[5] In the same way, Pt/C-PPy-Pol was also prepared by using C-PPy instead of F-C and following the polyol process.

TABLE 1: Summary of the Catalysts and Preparation Strategies Adopted for the Study

catalyst designation	support composition	process of Pt dispersion
Pt/C-PPy-Pre	Vulcan XC-72 + PPy	preprecipitation
Pt/C-Pre	Vulcan XC-72	preprecipitation
Pt/C-Pol	Vulcan XC-72	polyol
Pt/C-PPy-Pol	Vulcan XC-72 + PPy	polyol

The details of the catalyst systems prepared in this study are summarized in Table 1.

2.2. Fabrication of Membrane Electrode Assembly (MEA). Both anode and cathode comprised a backing layer, a gas diffusion layer (GDL), and a reaction layer. Teflonized carbon paper with a thickness of 0.35 mm was used as the backing layer in the electrodes. To prepare the gas diffusion layer, a mixture of 15 wt % polytetrafluoroethylene (PTFE) and Vulcan XC-72 carbon was suspended in cyclohexane and homogenized using an ultrasonic processor for 1 min. The resultant slurry was brush-coated on the teflonized carbon paper and sintered in a furnace at 350 °C for 30 min. To prepare the catalyst layer, a mixture of the required amount of catalyst and Nafion (30% of platinum) in isopropyl alcohol was sonicated for 1 min, and the resulting slurry was applied on the GDL by the brush-coating method. An identical Pt loading of 0.5 mg cm^{-2} (active area 5 cm^2) was maintained in the cathode and anode for all the MEAs. A thin layer of 5 wt % Nafion solution was spread on the surface of each electrode to ensure sufficient ionomer contact with the catalyst surface. For membrane pretreatment, Nafion 212 (DuPont) membrane was boiled with 3 wt % H_2O_2 for 1 h followed by boiling with DI water for an additional 1 h. Subsequently, the membrane was boiled with 0.5 M H_2SO_4 for 1 h followed by boiling for 1 h in DI water. The MEA was obtained by hot-pressing the cathode and anode on either side of the pretreated Nafion 212 membrane at 0.5 ton pressure and 130 °C for 90 s.

2.3. Material Characterization. The structure and morphology of the electrocatalysts were analyzed using a high-resolution transmission electron microscope (HR-TEM) Tecnai-T 30 model at an accelerated voltage of 300 kV. The samples for TEM were prepared by placing a drop of the catalyst sample in isopropanol onto a carbon-coated Cu grid. X-ray diffraction (XRD) was recorded on an Xpert Highscore Plus instrument using Cu−K_α radiation at a step of 0.02° (2θ). The Scherrer and Bragg formulas were employed to calculate the mean crystalline size and the lattice parameter of the catalysts. X-ray photoelectron spectroscopic (XPS) measurements were carried out on a VG Micro Tech ESCA 300° instrument at a pressure of $>1 \times 10^{-9}$ Torr (pass energy of 50 eV, electron take off angle 60°, and the overall resolution was ~0.1 eV). Surface area and pore size were characterized using a Quantachrome Instrument.

2.4. Cyclic Voltammetry and Rotating Disk Electrode Analysis. The electrochemical properties of the catalysts were measured by cyclic voltammetric (CV) and rotating disk electrode (RDE) analysis using an Autolab PGSTAT30 (Eco-Chemie) instrument in a conventional three-electrode test cell with a normal hydrogen electrode (NHE) and platinum foil as the reference and counter electrodes, respectively. For preparing the working electrode, after polishing the glassy carbon (GC) electrode using 0.3 and 0.05 μm alumina slurries, a 10 μL aliquot of the catalyst slurry made by sonicating 10 mg of catalyst in 1 mL of 3:2 ethanol−water mixture was drop-coated on the electrode surface. Subsequently, 2 μL of 0.01 wt % Nafion diluted with ethanol was applied on the whole surface of the electrode to yield a uniform thin film. This electrode was then dried in air and was used as the working electrode for all electrochemical studies. An aqueous solution of 0.5 M H_2SO_4 was used as the electrolyte for normal CV and RDE studies. Kinetics of ORRs of all the catalyst were studied by using an RDE, possessing a platinum loading in the working electrode of 0.14 mg cm^{-2}, in 0.5 M H_2SO_4 using a three-electrode cell assembly at a scan rate of 10 mV/s at 400, 900, 1200, 1600, and 2500 rpm.

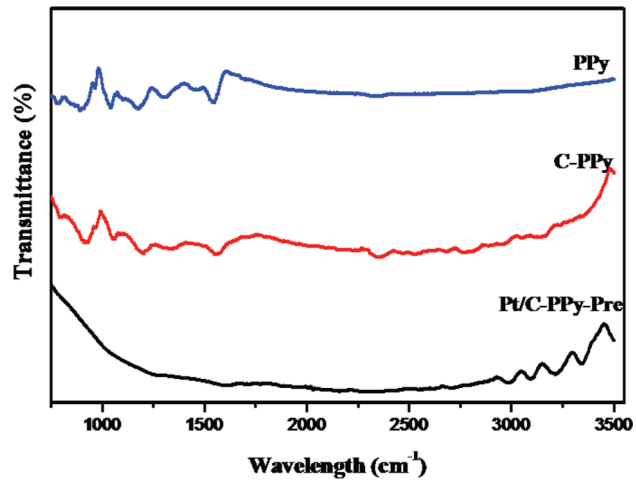

Figure 1. FT-IR spectra of PPy, C-PPy, and Pt/C-PPy-Pre.

2.5. Single Cell Performance Analysis. Single cell fuel cell analyses of MEAs were done by an Arbin fuel cell test station (model Arbin-001 MITS Pro-FCTS 5.0-FCTS) at 60 °C. A single cell had an area of 5 cm^2 with serpentine flow fields (Electrochem, Inc.). Polarization measurements were conducted with a flow of 0.2 slpm and 100% humidified H_2, O_2, and air.

Results and Discussion

The existence of PPy formed by the adopted in situ polymerization route has been confirmed by Fourier transform infrared (FT-IR) and thermogravimetric analysis (TGA). FT-IR can provide rich information about the functional groups grafted onto the CB surface. FT-IR spectra of PPy, C-PPy, and Pt/C-PPy-Pre are presented in Figure 1. The peaks at 1537 and 1446 cm^{-1} correspond to the symmetric and asymmetric ring stretching vibration modes of PPy. Furthermore, the peaks at 1040 and 1296 cm^{-1} are the C−H deformation vibration and the −C−N stretching vibration, respectively. The presence of PPy on carbon has been reflected through the characteristic signatures of the species. The two peaks present in the spectrum of C-PPy at 1552 and 1326 cm^{-1} can be attributed to the symmetric and asymmetric ring stretching vibration of the pyrrole ring.[23] Peaks at 1198 and 1048 cm^{-1} are the −C−N stretching and −C−H deformation vibration, respectively.[24] Less intense peaks in the case of Pt/C-PPy-Pre at 1572 and 1256 cm^{-1} are attributed to the symmetric ring stretching mode of the pyrrole ring and the C−N stretching vibration, respectively.

TGA profiles shown in the Figure 2 compare the thermal decomposition of PPy, C-PPy, and Pt/C-PPy-Pre. Weight loss from 100 to 200 °C in all the three materials is expected to be due to the loss of water content in the samples. PPy starts to decompose at 200 °C as evident from the figure. C-PPy composite also displays a small weight loss starting from 200 °C due to the decomposition of the PPy moiety in the sample. Sharp weight loss at 600 °C in the composite is due to the oxidation of carbon. The broad nature of the weight loss profile of PPy grafted on carbon, in comparison to that of the pristine

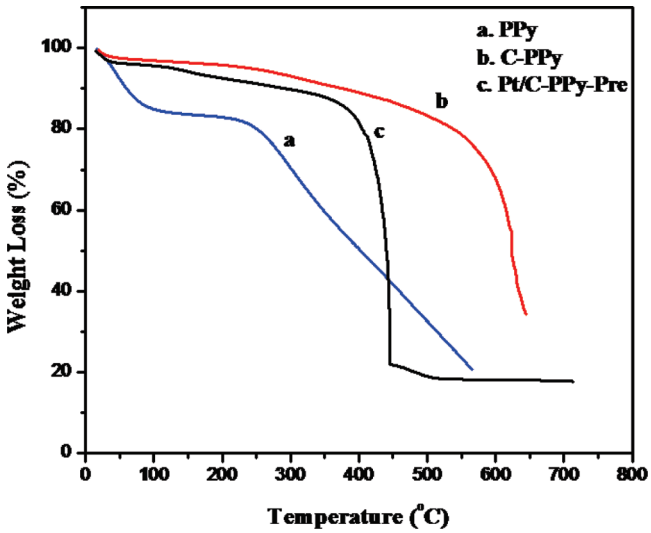

Figure 2. TGA results of PPy, C-PPy, and Pt/C-PPy-Pre at a heating rate of 10 °C per minute to 800 °C in air atmosphere.

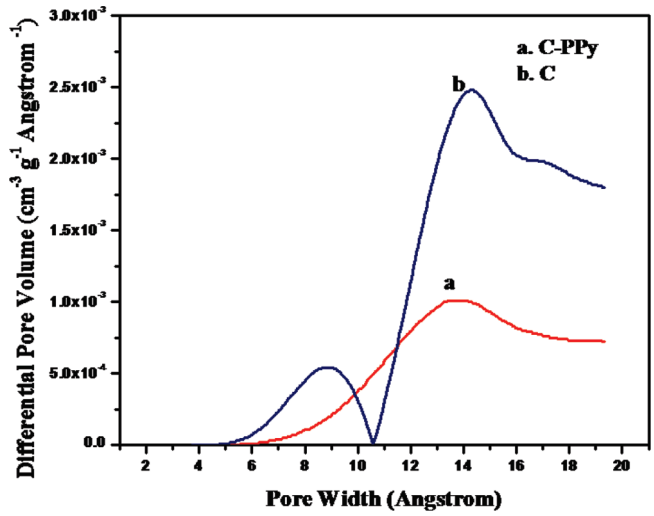

Figure 3. Curves of pore size distribution of C-PPy and Vulcan XC 72.

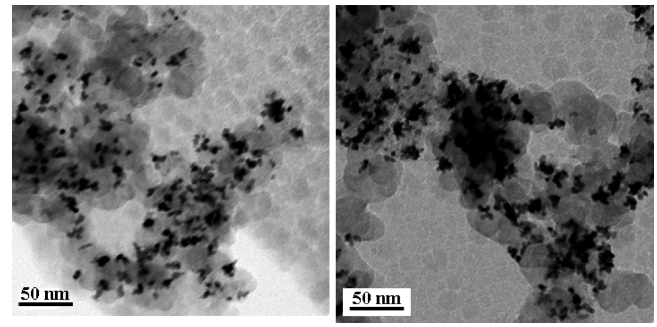

Figure 4. HR-TEM of Pt/C-PPy-Pre.

PPy sample, indicates enhancement in the stability of PPy when it is formed on the relatively thermally stable grains of Vulcan XC.[20] In Pt/C-PPy-Pre, the weight loss at 200 °C due to the decomposition of PPy is not visible enough, probably due to the additional stability gained by PPy in the presence of the dispersed Pt nanoparticles along the polymer matrix. Unlike C-PPy, where carbon shows a gradual weight loss from 600 °C, carbon in Pt/C-PPy-Pre shows fast and relatively low temperature decomposition (400 °C). Since Pt can facilitate oxidation, a fast decomposition of the Pt-decorated surface can be expected. Further, the residue content of 19% is the amount of Pt present in the composite.

The N_2 adsorption−desorption isotherm reveals the presence of micro- and mesopores in the adsorbents. Brunauer−Emmett−Teller (BET) surface area values display a significant fall from 206 $m^2\ g^{-1}$ in the case of Vulcan XC-72 to 61 m^2/g after the in situ polymerization. This is strong evidence of surface polymerization of the carbon substrate with PPy because the pores present on the surface are filled and covered by PPy with a progressive decrease in the surface area as well as the nitrogen uptake. Figure 3, which shows pore size distribution of Vulcan XC and C-PPy, clearly demonstrates that the differential pore volume of Vulcan XC-72 decreases by 58% (from 0.086 to 0.025 $cm^3\ g^{-1}$) after the composite formation. The figure gives a clear indication of effective coverage or filling of micro- and mesopores present on the surface of carbon by PPy.[25,26] However, even after the polymerization process, the system retains some extent of micro- and mesopore characteristics as evident from the differential pore volume profile. In this way, we could utilize the CP phase as a means to smoothen the carbon surface by effectively filling a significant amount of micro- and mesopores, which generally make an adverse contribution to the achievement of high Pt utilization. The relatively smooth surface of the composite system obtained by the aforementioned strategy helps Pt nanoparticles to disperse uniformly on the composite with improved adhesion on the surface by the intervention of the thin PPy layer formed on the carbon support surface.

TEM images of Pt/C-PPy-Pre as shown in Figure 4 reveal the presence of well-dispersed Pt particles on the surface of C-PPy with a size distribution of 6−8 nm. The relatively large Pt size distribution can be accounted for on the basis of the decrease in the surface area of the carbon support by the filling of pores with PPy, as illustrated in the previous section. Figure S1 (Supporting Information) shows the XRD patterns of F-C, C-PPy, and Pt/C-PPy Pre. The broad peak at 2θ around 25° obtained in the case of F-C, which is attributed to the (002) plane of carbon, does not change its nature after the in situ polymerization (C-PPy). This more or less identical behavior of the carbon plane indicates that, after the formation of PPy composite, neither the crystalline nature of the carbon substrate is reduced, nor is excess amorphous character of PPy generated on the surface. The XRD patterns of the Pt/C-PPy-Pre show strong diffractions at around 2θ 40.1°, 46.4° and 67.7°, which can be indexed as platinum (111), (200), and (220) reflections, respectively, indicating that the catalysts have face-centered cubic (fcc) structure.[27] The average Pt particle size estimated from the (220) reflection of Pt using Scherrer equation is 6 nm, which is almost similar to the estimated size from the TEM images.

X-ray photoelectron spectra (XPS) for Pt/C-Pol and Pt/C-PPy-Pre overarching the Pt (4f) region are shown in Figure S2. For Pt/C-Pol, the binding energies of Pt ($4f_{7/2,5/2}$) are observed at 71.39 and 74.64 eV, respectively, indicating Pt^0 state. Also, there is no indication of oxidized Pt component. On the other hand, Pt/C-PPy-Pre shows Pt (4f) peaks shifted into higher binding energy as compared to Pt^0 peaks, and, accordingly, Pt (4f) peaks are resolved into two sets of spin−orbit doublets. Indeed, significant peaks are observed due to $Pt^{\delta-}$ ($4f_{7/2,\ 5/2}$) at 72.8 and 77.13 eV and Pt^0 ($4f_{7/2,\ 5/2}$) at 71.4 and 74.93 eV, respectively. Similar oxidation states on $Au^{\delta-}$ and $Ag^{\delta-}$ are reportedly known.[28] The peaks correspond to the oxygen, nitrogen, and carbon are also shown in Figure 5.

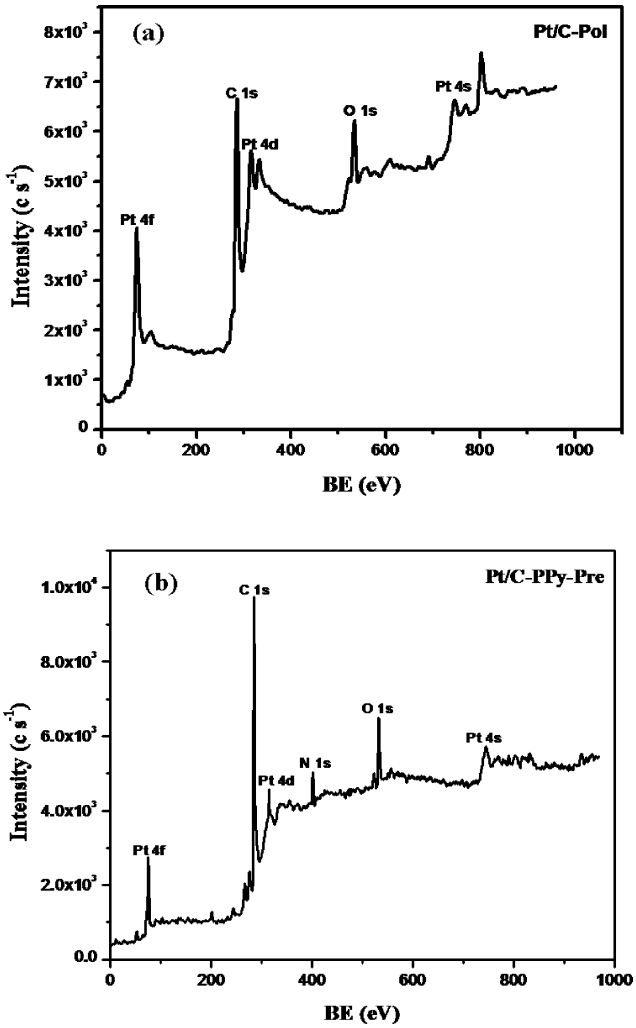

Figure 5. XPS spectra of (a) Pt/C-Pol and (b) Pt/C-PPy-Pre with core levels of C1s, O1s, N1s, and Pt 4f.

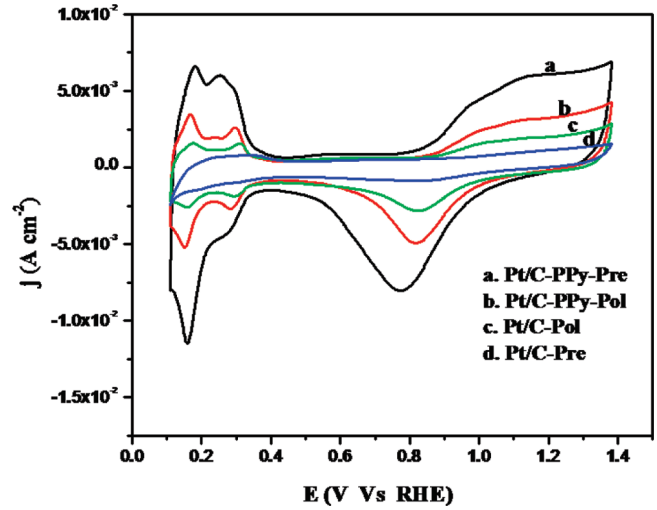

Figure 6. Superimposed cyclic voltammograms of Pt/C-PPy-Pre, Pt/C-PPy-Pol, and Pt/C-Pol coated on a 3 mm diameter GC tip in 0.5 M H_2SO_4 using RHE as the reference electrode and Pt foil as the counter electrode at room temperature; sweep rate is 50 mV s^{-1}.

Cyclic voltammograms of Pt/C-Pol, Pt/C-PPy-Pol, Pt/C-Pre, and Pt/C-PPy-Pre in 0.5 M H_2SO_4 at a scan rate of 50 mV s^{-1} are presented in Figure 6. The CV features resemble that of a polycrystalline Pt electrode in acid solution.[29] In the cyclic voltammograms, the H_2 region appeared in the potential range of 0.11−0.36 V vs RHE, and oxygen reduction shows a peak current density at 0.8 V vs RHE for all the four catalysts. The electroactive surface area (ESA) of Pt has been evaluated from the electric charge for the desorption of H_2 (Q_H) (assuming that $Q_H = 0.210$ mC/cm^2 for a smooth polycrystalline Pt).[30] The Pt/C-PPy-Pre shows an active area of 63 m^2 (g-Pt)$^{-1}$. As evident from the figure, ESA decreases dramatically by changing the preparation method as well as the support materials. The calculated values of ESA of the systems are summarized in Table 2. From Figure 6, Pt/C-Polyol and Pt/C-Pre display significantly low ESA compared to Pt/C-PPy-Pre because a major part of the formed platinum nanoparticles in the former two cases goes into the micro- and mesopores present in the carbon substrate. During the preparation of electrodes, there are limitations to establish enough contact with these Pt nanoparticles and ionomer, leading to the anticipated reduction in the active Pt area. On the other hand, Pt dispersion on the composite support shows a better result because around 60% of the pores are preferentially blocked by using PPy, and, consequently, passage of Pt in the geometrically restricted areas could be prevented to a large extent. Furthermore, by adopting the preprecipitation method, where most of the Pt ions initially give a precipitation of $(NH_4)_2PtCl_6$ on the surface of the composites and subsequently reduce to Pt using the reducing agent, penetration of the precipitate into the smaller pores is unlikely. Therefore, the present strategy gives better active Pt area and, thereby, improved Pt utilization level, even though the preprecipitation route leads to the deposition of Pt particles on the composite surface with size 2.5 times higher than that of the particles deposited on the carbon by the polyol process.

Generally, the CP-based systems are reportedly prone to fast deactivation owing to the catastrophic morphological changes due to swelling-drying cycle and drastic electrochemical environment changes under the testing conditions. In Figure S3 we have displayed the change in EAS of 20 wt % Pt/C-PPy-Pre in 0.5 M H_2SO_4 acid medium as a function of number of cycles from the normal CV analysis at the rate of 50 mV s^{-1}. Interestingly, there is no appreciable change in the EAS during this potential and duration of cycling. The PPy layer, which is already very thin, might have secured additional structural stability due to the rigid carbon core, and the Pt nanoparticles might be anchored more strongly on the substrate surface due to the intervention of the PPy layer on the surface. Thus a controlled interplay by the characteristic features of the individual phases might have created a novel system with balanced properties well-suited to meet the critical requirements of high Pt utilization and durability.

A hydrodynamic voltammogram for the ORR using an RDE at 1200 rpm on the catalysts Pt/C-PPy-Pre, Pt/C-PPy-Pol, and Pt/C-Pol electrodes is shown in Figure 7. The ORR voltammogram shows three different regions: the kinetic control region, the diffusion limited region, and the mixed control region. The more positive onset potential of the modified catalyst shows that the ORR on Pt/C-PPy-Pre is relatively fast compared to that on Pt/C-PPy-Pol and Pt/C-Pol. The half-wave potential of the modified catalyst shows a positive shift of 0.025 V compared to that of Pt/C-PPy-Pol and a more significant shift of 0.067 V compared to that of Pt/C-Pol. Similarly, the limiting current density, j_{lim}, at the Pt/C-PPy-Pre electrode is higher by 2 mA cm^{-2} and 2.2 mA cm^{-2} compared to that of Pt/C-PPy-Pol and Pt/C-Pol, respectively. The favorable shifts in the onset, half-wave, and limiting current regions of the voltammogram

TABLE 2: Electrochemical Characteristics of ORR of Catalysts

catalyst name	active Pt area, EAS (m^2 g-Pt^{1-})	current density at 0.85 V (mA cm^{-2})	mass activity at 0.85 V (A g^{-1})	kinetic current density (j_k) at 0.58 V (mA cm^{-2})
Pt/C-PPy-Pre	64.29	-2.41×10^{-3}	17.02	185.18
Pt/C-PPy-Pol	24.49	-1.47×10^{-3}	10	51.70
Pt/C-Pol	11.28	4.91×10^{-4}	3.46	25.37

corresponding to the electrode of Pt/C-PPy-Pre can be accounted for by the improved ORR activity on the modified catalyst.

A Tafel plot derived from the hydrodynamic voltammogram at an electrode rotation of 1200 rpm is shown in Figure S4. This polarization plot has been corrected for diffusion effect using the following equation:[31,32]

$$j_k = \frac{j_L J}{j_L - j}$$

where j_k is the kinetic current density, j_L is the limiting current density, and j is the measured current density. This equation is valid only when the reaction follows first-order kinetics. Pt/C-PPy-Pre has a Tafel slope of -81 mV dec^{-1} in comparison to -80 and -87 mV dec^{-1} obtained for Pt/C-PPy-Pol and Pt/C-Pol, respectively. The Tafel slope is an indication of the mechanism of the electrode reaction, which is related to the change in the nature of adsorbed oxygen species and their coverage variation with the potential. The low current density region corresponds to the oxygen reduction when the adsorbed hydroxyl species at the Pt surface determines the electrode activity. The comparatively high Tafel slope of Pt/C-Pol is probably due to the inefficient converge of the adsorbed intermediates, which leads to a decrease in the rate of the ORR. On the other hand, both of the surface-modified catalysts show almost the same Tafel slopes, indicating a similar adsorption mechanism and coverage of the adsorbed species responsible for the reduction reaction.

The Koutecky−Levich plot, i.e., a plot of the inverse of current density ($1/j$) as a function of the inverse of the square root of the rotation rate ($\omega^{-1/2}$), is a useful method to compare the electrochemical performance of different electrocatalysts. The Koutecky−Levich analysis accounts for the total current

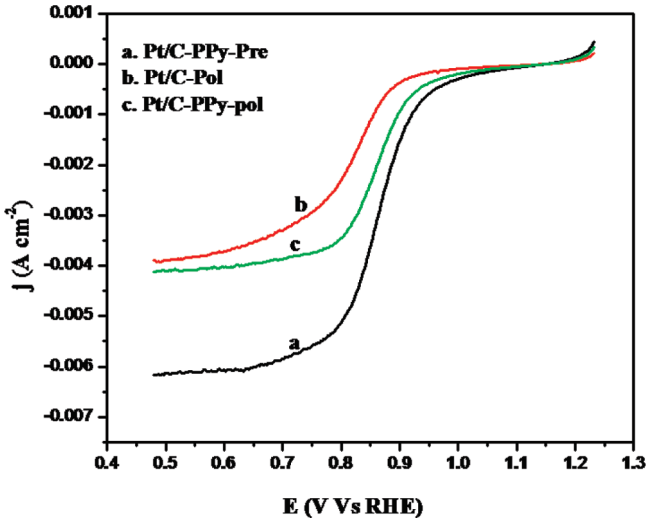

Figure 7. Hydrodynamic voltammogram curves obtained with an RDE for the ORR on Pt/C-PPy-Pre, Pt/C-PPy-Pol, and Pt/C-Pol in O_2-saturated 0.5 M H_2SO_4 at a sweep rate of 10 mV s^{-1}.

during the oxygen reduction in terms of both the diffusing part and the kinetic part, and could be expressed as follows:

$$\frac{1}{j} = \frac{1}{j_k} + \frac{1}{j_d} + \frac{1}{j_f} \quad (1)$$

where j represents the disk electrode current density, j_d is the diffusion-limited current density owing to the mass transport, and j_k is the kinetic current density determined by the charge transfer. The film diffusion current density (j_f) in the present case can be neglected a,s the amount of Nafion is significantly low and hence not expected to be a factor in the limiting current density.[33,34] In the laminar flow region, the diffusion current density is a function of the rotational velocity, and hence the above equation may be approximated as follows:

$$\frac{1}{j} = \frac{1}{nFkC_{O_2}} + \frac{1}{0.62nFAC_{O_2}D_{O_2}^{2/3}v^{-1/6}\omega^{1/2}} \quad (2)$$

where k is the reaction rate constant, n is the number of electrons exchanged per O_2 molecule, F is the Faraday constant, A is the electrode geometric area, C_{O2} is the bulk oxygen concentration (1.22×10^{-6} mol cm^{-3}), D_{O2} is the diffusion coefficient of molecular oxygen (1.04×10^{-5} cm^2 s^{-1}), ν is the kinematic viscosity of the electrolyte (0.01009 cm^2 s^{-1}), and ω is the electrode rotation speed in radians per second ($= 2\pi f = 2\pi$ rpm number/60). The plot of $1/j$ vs $\omega^{-1/2}$ gives a linear relation with a Y-intercept equal to the inverse of the kinetic current ($1/j_k$). Accordingly, Figure 8 shows the Koutecky−Levich plots for O_2 reduction at Pt/C-PPy-Pre and Pt/C-PPy-Pol, Pt/C-Pol electrodes at a potential of 0.58 V vs RHE. Analysis of the Y-intercepts gives a practical way to determine the kinetic current density (j_k) values at each potential. As evident from the Koutecky−Levich plots in Figure 8a, the Pt/C-PPy-Pre leads to higher j_k values compared to the other systems; the respective j_k values are shown in Table 2. The improved ORR kinetics on the Pt/C-PPy-Pre system is clearly visible from the respective polarization profile. For example, at 0.8 V, the j_k value of the Pt/C-PPy-Pre is 1.5 and 2.5 times higher than that of Pt/C-PPy-Pol and Pt/C-Pol, respectively. Furthermore, the current density and mass activity characteristics for the ORR at the kinetic control region (i.e., potential greater than 0.8 V) have been evaluated. Compared with Pt/C-Pol and Pt/C-PPy-Pol, the greater current density and mass activity of the ORR on Pt/C-PPy-Pre at 0.85 V (Table 2) reveal that the electroactivity of the ORR on Pt/C-PPy-Pre is greater than that of the rest. The current density and mass activity of the ORR on Pt/C-PPy-Pre are 4.9 and 5 times higher than that of Pt/C-Pol and 3.2 and 1.7 times higher than that of Pt/C-PPy-Pol, respectively. The higher electroactivity of ORR on Pt/C-PPy-Pre can be attributed to the higher dispersion of Pt nanoparticles, improved interaction of the nanoparticle with support, and shorter Pt−Pt interatomic distance caused by the presence of a hetroatom (nitrogen) in the support.[7,35−37] The higher ORR activity of the Pt-based alloy

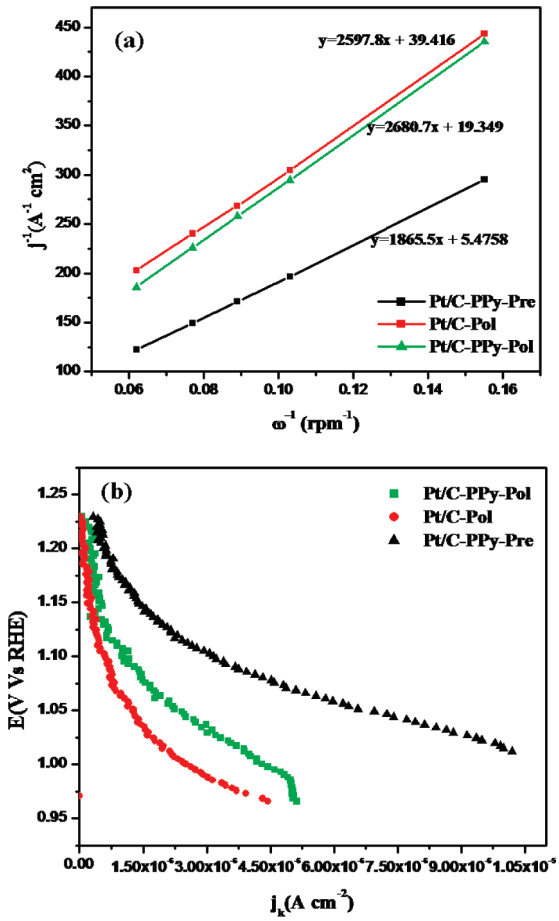

Figure 8. (a) Koutecky−Levich plots obtained from RDE studies in O_2-saturated 0.5 M H_2SO_4 for Pt/C-PPy-Pre, Pt/C-PPy-Pol, and Pt/C-Pol at a potential of 0.58 V. Sweep rate: 10 mV s^{-1}. (b) Kinetic current values obtained from the Koutecky−Levich plots of the three catalysts are plotted against potential values.

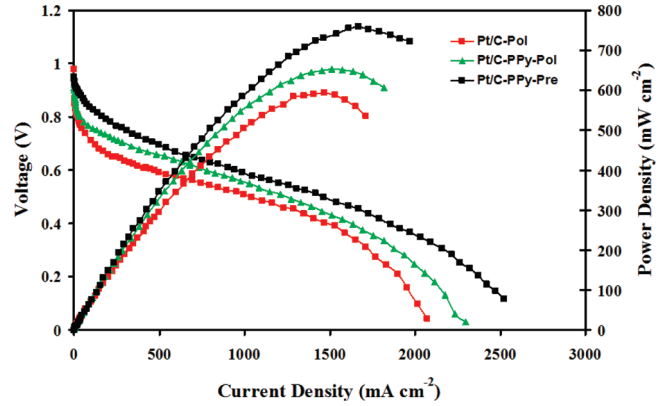

Figure 9. *I*−*V* curves of PEMFCs with Pt/C-PPy-Pre, Pt/C-PPy-Pol, and Pt/C-Pol as the cathode catalyst layers. Platinum (0.5 mg cm^{-2}) was present in both the cathode and the anode, and Nafion 212 was used as the polymer electrolyte membrane. Test conditions: Cell operated at 60 °C, H_2 and O_2 flow rate is 0.2 slpm, and 100% humidified H_2 and O_2 were used at atmospheric pressure.

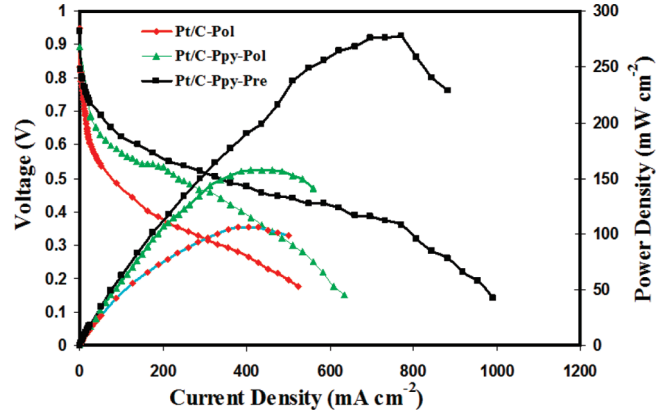

Figure 10. *I*−*V* curves of PEMFCs with Pt/C-PPy-Pre, Pt/C-PPy-Pol, and Pt/C-Pol as the cathode catalyst layers. Platinum (0.5 mg cm^{-2}) was present in both the cathode and the anode, and Nafion 212 was used as the polymer electrolyte membrane. Test conditions: Cell operated at 60 °C, H_2 and air flow rate is 0.2 slpm,and 100% humidified H_2 and air were used at atmospheric pressure.

catalyst is generally correlated to the change in Pt−Pt interatomic distance.[38]

Kinetic current values obtained from RDE analysis are plotted against the corresponding potentials to analyze current−potential behavior of different catalysts, as shown in Figure 8b. The higher performance of Pt/C-PPy-Pre catalyst is clearly visible from the figure. At higher potentials, the activation loss for the ORR is about 2 times less compared to that of the catalyst prepared by the polyol method. These results emphasize that the N_2 content in the polymer not only prevents platinum particle agglomeration but also promotes the catalytic activity of platinum nanoparticle. The catalytic activity of N_2-containing systems such as carbon nanotubes and graphene toward the ORR has been reported.[1,2]

Polarization curves of the MEA based on Pt/C-PPy-Pre, Pt/C-PPy-Pol, and Pt/C-Pol as cathode catalysts are shown in Figure 9. Even though all three systems display more or less similar open circuit voltage values, a significant performance enhancement in the three prominent polarization regions of activation, ohmic, and mass transfer can be seen with the MEA fabricated with Pt/C-PPy. Especially, the higher performance in the activation-controlled region of the modified catalyst further confirms the improved oxygen reduction activity of this system, which has been already revealed through the RDE studies. Current densities of the catalysts at 0.6 V are 0.94, 0.78, and 0.45 A cm^{-2} for Pt/C-PPy-Pre, Pt/C-PPy-Pol, and Pt/C-Pol, respectively. Further, the overall enhancement in the current−voltage response characteristics by the modified systems has helped this MEA to attain the highest power density of (760 mW cm^{-2}) compared to that with the other two systems. Figure 10 shows the fuel cell performance of these three catalysts using air feed in the cathode side. The modified catalyst system displays a maximum current density of 1 A cm^{-2} and a power density of 260 mW cm^{-2}, which is higher than the rest of the catalysts. The enhanced performance characteristics observed with the MEA containing Pt/C-PPy-Pre in the presence of oxygen or air as the cathode feed shows that, in the modified catalyst, as more Pt particles are active to facilitate the electrode reactions, the system could respond quite well compared to the other two systems, as the test station gradually drags higher current from the cell.

4. Conclusion

PPy/Vulcan XC-72 hybrid material was prepared by in situ chemical oxidative polymerization of pyrrole monomer on carbon. Solid confirmation for the formation of PPy on Vulcan XC-72 was obtained from FT-IR, TGA, and surface area analyses. The controlled polymerization helped to preferentially block a significant amount of micro- and mesopores, which otherwise would act as pockets where significant a amount of Pt particles could be buried, leading to a reduction in Pt

utilization. Furthermore, by adopting a preprecipitation route to disperse Pt nanoparticles, selective dispersion of Pt nanoparticles on the PPy-modified surface could be achieved. Even though this approach gave Pt particles with a size approximately 2 times higher than the one prepared by the polyol process, the new system showed significantly high electractive surface area and performance characteristics owing to the higher Pt utilization level. The kinetic current densities (j_k) measured at different potentials from the Koutecky−Levich plots were appreciably higher on the modified catalyst compared to that on Pt decorated on Vulcan XC-72 by both polyol and preprecipitation methods. Enhancement in current density as well as power density of the modified catalyst using both pure oxygen and air feed underlines the improved ORR activity of this system compared to the other catalysts. The polymer covering of the support helps to improve proton and electron transport and to maximize the TPB, whereas the heteroatom present in the polymer assisted in reducing the Pt−Pt interatomic distance and consequently enabling high platinum utilization. On the other hand, the preprecipitation method prevents the passage of nanoparticles into the micro- and mesopores present on the surface due to the formation of colloids during the preparation. Thus, the present study reveals the importance of modification of the catalyst support as well as different preparation methods for enhancing catalytic activity and platinum utilization for PEMFCs.

Acknowledgment. This work is supported by the Council of Scientific and Industrial Research (CSIR), Govt. of India, under Network Project No. NWP0022. The authors thank Dr. S. Sivaram for continuous encouragement. S.M.U. gratefully acknowledges CSIR, New Delhi, for the award of junior research fellowship.

Supporting Information Available: Figures showing XRD of the catalyst, XPS of Pt in Pt/C-Pol and Pt/C-PPy-Pre, cycle-dependent voltammetric durability analysis, and Tafel plot. This material is available free of charge via the Internet at http://pubs.acs.org.

References and Notes

(1) Gong, K.; Du, F.; Xia, Z.; Durstock, M.; Dai, L. *Science* **2009**, *323*, 760–764.
(2) Wang, Y.; Shao, Y.; Matson, D. W.; Li, J.; Lin, Y. *ACS Nano* **2010**, *4*, 1790–1798.
(3) Winther-Jensen, B.; Winther-Jensen, O.; Forsyth, M.; MacFarlane, D. R. *Science* **2008**, *321*, 671–674.
(4) Li, W.; Wang, X.; Chen, Z.; Waje, M.; Yan., *Langmuir* **2005**, *21*, 9386–9389.
(5) Wee, J.-H.; Lee, K.-Y.; Kim, S. H. *J. Power Sources* **2007**, *165*, 667–677.
(6) Limjeerajarus, N.; Yanagimoto, T.; Yamamoto, T.; Ito, T.; Yamaguchi, T. *J. Power Sources* **2008**, *185*, 217–221.
(7) Bollepalli, S. U.S. Patent 7, 390441 B2, 2008.
(8) Wu, G.; Chen, Y.-S.; Xu, B.-Q. *Electrochem. Commun.* **2005**, *7*, 1237–1243.
(9) Balan, B. K.; Unni, S. M.; Kurungot, S. *J. Phys. Chem. C* **2009**, *113*, 17572–17578.
(10) Zhao, H.; Li, L.; Yang, J.; Zhang, Y. *J. Power Sources* **2008**, *184*, 375–380.
(11) Stevens, D. A.; Dahn, J. R. *Carbon* **2005**, *43*, 179–188.
(12) Roen, L. M.; Paik, C. H.; Jarvi, T. D. *Electrochem. Solid-State Lett.* **2004**, *7*, A19–A22.
(13) Antolini, E.; Gonzalez, E. R. *Solid State Ionics* **2009**, *180*, 746–763.
(14) Orilall, M. C.; Matsumoto, F.; Zhou, Q.; Sai, H.; Abruña, H. D.; DiSalvo, F. J.; Wiesner, U. *J. Am. Chem. Soc.* **2009**, *131*, 9389–9395.
(15) Wallace, G. G.; Innis, P. C. *J. Nanosci. Nanotechnol.* **2002**, *2*, 441–451.
(16) Youqing, S.; Meixiang, W. *J. Polym. Sci. A: Polym. Chem.* **1999**, *37*, 1443–1449.
(17) Huang, J. H.; Kaner, R. B. *Chem. Commun.* **2006**, 367–376.
(18) Bashyam, R.; Zelenay, P. *Nature* **2006**, *443*, 63–66.
(19) Martínez Millán, W.; Toledano; Thompson, T.; Arriaga, L. G.; Smit, M. A. *Int. J. Hydrogen Energy* **2009**, *34*, 694–702.
(20) Mokrane, S.; Makhloufi, L.; Alonso-Vante, N. *J. Solid State Electrochem.* **2008**, *12*, 569–574.
(21) Jiwei, L.; Jingxia, Q.; Miao, Y.; Chen, J. *J. Mater. Sci.* **2008**, *43*, 6285–6288.
(22) Liu, C.; Xue, X.; Lu, T.; Xing, W. *J. Power Sources* **2006**, *161*, 68–73.
(23) Feng, X.; Huang, H.; Ye, Q.; Zhu, J.-J.; Hou, W. *J. Phys. Chem. C* **2007**, *111*, 8463–8468.
(24) Zhang, X.; Zhang, J.; Song, W.; Liu, Z. *J. Phys. Chem. B* **2005**, *110*, 1158–1165.
(25) Choi, Y. S.; Joo, S. H.; Lee, S.-A.; You, D. J.; Kim, H.; Pak, C.; Chang, H.; Seung, D. *Macromolecules* **2006**, *39*, 3275–3282.
(26) Saha, D.; Deng, S. *Langmuir* **2009**, *25*, 12550–12560.
(27) Tang, Z.; Geng, D.; Lu, G. *Mater. Lett.* **2005**, *59*, 1567–1570.
(28) Hirakawa, T.; Kamat, P. V. *J. Am. Chem. Soc.* **2005**, *127*, 3928–3934.
(29) Susut, C.; Chapman, G. B.; Samjeske, G.; Osawac, M.; Tong, Y. *Phys. Chem. Phys.* **2008**, *10*, 3712–3721.
(30) Kim, H.-J.; Kim, D.-Y.; Han, H.; Shul, Y.-G. *J. Power Sources* **2006**, *159*, 484–490.
(31) Gojkovic, S. L.; Zecevic, S. K.; Savinell, R. F. *J. Electrochem. Soc.* **1998**, *145*, 3713–3720.
(32) Elezovic, N. R.; Babic, B. M.; Gajic-Krstajic, L.; Radmilovic, V.; Krstajic, N. V.; Vracar, L. J. *J. Power Sources* **2010**, *195*, 3961–3968.
(33) Lawson, D. R.; Whiteley, L. D.; Martin, C. R.; Szentirmay, M. N.; Song, J. I. *J. Electrochem. Soc.* **1988**, *135*, 2247–2253.
(34) Watanabe, M.; Igarashi, H.; Yosioka, K. *Electrochim. Acta* **1995**, *40*, 329–334.
(35) Maldonado, S.; Stevenson, K. J. *J. Phys. Chem. B* **2005**, *109*, 4707–4716.
(36) Shao, Y.; Sui, J.; Yin, G.; Gao, Y. *Appl. Catal. B: Environ.* **2008**, *79*, 89–99.
(37) Wu, G.; Dai, C.; Wang, D.; Li, D.; Li, N. *J. Mater. Chem.* **2009**, *20*, 3059–3068.
(38) Lee, M. H.; Do, J. S. *J. Power Sources* **2009**, *188*, 353–358.

JP104664T